

# The impact of memory on learning sequence-to-sequence tasks

Alireza Seif<sup>1</sup>, Sarah A.M. Loos<sup>2</sup>, Gennaro Tucci<sup>3</sup>, Édgar Roldán<sup>2</sup> and Sebastian Goldt<sup>†4</sup>

<sup>1</sup>Pritzker School of Molecular Engineering, University of Chicago, USA

<sup>2</sup>ICTP – The Abdus Salam International Centre for Theoretical Physics, Trieste, Italy

<sup>3</sup>Max Planck Institute for Dynamics and Self-Organization, Göttingen, Germany

<sup>4</sup>International School of Advanced Studies (SISSA), Trieste, Italy

## Abstract

The recent success of neural networks in machine translation and other fields has drawn renewed attention to learning sequence-to-sequence (seq2seq) tasks. While there exists a rich literature that studies classification and regression using solvable models of neural networks, learning seq2seq tasks is significantly less studied from this perspective. Here, we propose a simple model for a seq2seq task that gives us explicit control over the degree of memory, or non-Markovianity, in the sequences – the stochastic switching-Ornstein-Uhlenbeck (SSOU) model. We introduce a measure of non-Markovianity to quantify the amount of memory in the sequences. For a minimal autoregressive (AR) learning model trained on this task, we identify two learning regimes corresponding to distinct phases in the stationary state of the SSOU process. These phases emerge from the interplay between two different time scales that govern the sequence statistics. Moreover, we observe that while increasing the memory of the AR model always improves performance, increasing the non-Markovianity of the input sequences can improve or degrade performance. Finally, our experiments with recurrent and convolutional neural networks show that our observations carry over to more complicated neural network architectures.

## 1 Introduction

The recent success of neural networks on problems like machine translation and text summarisation has rekindled interest in tasks that require transforming a sequence of tokens into another sequence. Transformers [1] and other models for sequence-to-sequence (seq2seq) learning now also provide promising results in areas beyond natural language processing, such as symbolic regression [2–4], which were previously in the realm of genetic algorithms, and image captioning [5–7].

At the same time, these practical successes highlight the relative lack of theoretical understanding of learning seq2seq tasks with neural networks (NN), especially compared to the recent progress that was made on standard regression or classification tasks. There, a fruitful line of research focused on the importance of data structure for the success of neural networks. The idea there is to develop synthetic models of data and to analyse the dynamics and the performance of neural networks trained on that data. This approach was initiated in the early days of neural network theory, where data was modelled as random functions of Gaussian i.i.d. inputs, and the performance of a simple neural network, called the student, was studied [8–11]. The successes of neural networks in image classification [6, 12–14] then inspired a new generation of data models that take the effective low-dimensionality of images [15]

---

\*seif@uchicago.edu

†sgoldt@sissa.it

into account, such as object manifolds [16], the hidden manifold [17, 18], spiked covariates [19, 20], or low-dimensional mixture models embedded in high dimensions [21–23]. Meanwhile, other works focused on the impact of translation invariance [24–26]. By deriving learning curves for neural networks on these and other data models [27–30], these works clarified the role of data structure for the success of neural networks, for example by showing how the performance gap between neural networks and random features [31] is exacerbated by data with low intrinsic dimension [19, 21, 22, 32].

Since all these works consider classification or regression, the aforementioned recent successes of neural networks on seq2seq tasks make it an important challenge to extend this approach to this domain, too. What are key properties of sequences, akin to the low intrinsic dimension of images, that need to be modelled? How do these properties interact with different neural network architectures?

Here, we make a first step in this direction by proposing to use a minimal, solvable latent variable model for time-series data that we call the stochastic switching Ornstein-Uhlenbeck process (SSOU). The input data consists of a sequence  $\mathbf{x} = (x_t)_{t=0}^T$ , which depends on a latent, unobserved stochastic process  $\mathbf{c} = (c_t)_{t=0}^T$ . The learning task is to reconstruct the unobserved sequence  $\mathbf{c}$  from the input sequence  $\mathbf{x}$ , cf. fig. 1. The key data property we aim to describe and control is the *memory* within the input sequence  $\mathbf{x}$ . In the simplest scenario, the sequence  $x_t$  is memoryless: given the value of the present token  $x_t$ , the value of the next token  $x_{t+1}$  is statistically dependent solely on  $x_t$  but not on previous tokens  $x_{t' < t}$ . Such a sequence can be described by a Markov process. By tuning the dynamics of the latent process  $c_t$ , we can control the memory of the sequence, *i.e.* we can increase the statistical dependence of future tokens on their full history  $x_{t' < t}$  (we will introduce a precise, quantitative measure for the memory below). Adding memory thus makes the process non-Markovian and allows us to model richer statistical dependencies between tokens. At the same time, the presence of memory in a processes makes the mathematical analysis generally harder. Here, we use techniques introduced by Tucci *et. al.* [33] to show that statistical properties of the model such as its correlation functions, can be computed exactly even in the non-Markovian case and give important insights into the performance of various students trained on the reconstruction task.

We will contrast the memory of the sequence with the memory of various neural networks that we train on this task. We begin with a simple auto-regressive model, whose basic structure – one layer of weights followed by a non-linear activation function – makes it the seq2seq analogue of the famous perceptron model that has been the object of a large literature in the theory of neural networks focused on classification [8–11]. We also train simple convolutional (CNN) and (gated) recurrent neural networks (RNN) on the SSOU task. The memory of these students ranges from finite integration window in auto-regressive models and the kernel size of a CNN to the – in principle – unbounded memory of (gated) recurrent neural networks with internal hidden states [34].

The goal of our study is to understand the interplay between the memory of the data and the memory of the student when learning the seq2seq task  $\mathbf{x} \rightarrow \mathbf{c}$ . Our main contributions can be summarised as follows:

1. We introduce the stochastic switching Ornstein-Uhlenbeck process as a latent variable model for seq2seq tasks (section 2)
2. We describe how to tune the memory of the input and target sequences, and introduce a measure of non-Markovianity that quantifies this memory (section 4.1)
3. We identify two regimes in the performance of an auto-regressive model. These regimes correspond to distinct phases in the stationary state of the SSOU and they emerge from the interplay of two different time scales that govern the sequence statistics (section 4.2)
4. We show that the task difficulty is non-monotonous in the sequence memory for all three models

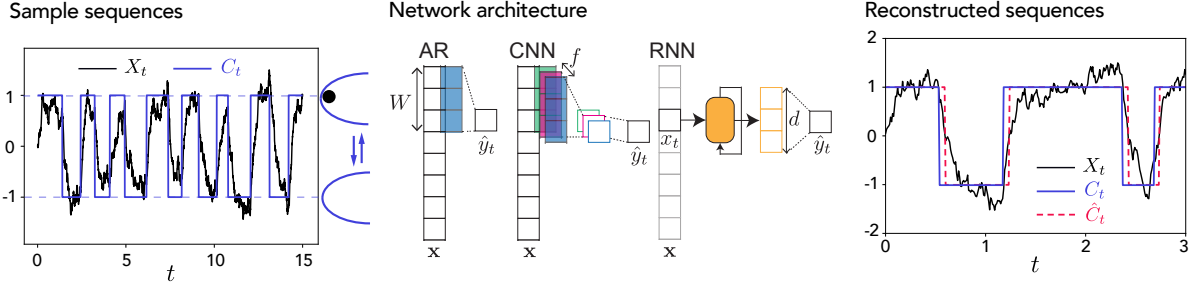


Figure 1: **A flexible, minimal model for sequence-to-sequence learning tasks with varying degrees of memory.** **Left:** The motion of a Brownian particle (black filled circle) in a switching parabolic potential “trap” yields dynamics as given by the SSOU (stochastic switching Ornstein Uhlenbeck) model given by eq. (1). Example trajectories for sequences of the particle’s position  $X_t$  (black line) and the trap center  $C_t$  (blue line) as shown as a function of time  $t$ . The blue dashed line is set at the trap centers  $C_0 = \pm 1$ . **Middle:** We train three types of models to reconstruct the trap positions  $C_t$  from the particle trajectories  $X_t$ : auto-regressive models (AR) as well as convolutional and recurrent neural networks (CNN and RNN, resp.) **Right:** Sample reconstruction of the particle trap positions  $\hat{y}_t$  (red dashed line) for one example input sequence ( $X_t$ , black solid line) compared with the actual hidden trap position ( $C_t$ , blue solid line). The sequence is a zoomed-in view of the sample sequence in the left panel. *Parameters:*  $\kappa = 10$ ,  $k = 1$ ,  $D = 0.5$ , simulation time step  $\Delta t = 0.02$ , AR model window size  $W = 2$ . For this example, we used 5000 training samples, evaluated them over 5000 test samples, a mini-batch size 32 and 5 epochs.

(auto-regressive, convolutional and recurrent): compared to the memoryless case, the task is harder with weak memory, but easier with strong memory. We explain the mechanism behind this effect in terms of the sequence statistics (section 4.3)

5. We finally find that increasing the memory of auto-regressive models and CNN improves their performance, while increasing the dimension of the memory of a gated RNN achieves only minimal improvements (section 4.3)

**Reproducibility** We provide code to sample from the SSOU model and reproduce our experiments at [https://github.com/alirezaseif/nonmarkovian\\_learning](https://github.com/alirezaseif/nonmarkovian_learning).

## 2 A model for sequence-to-sequence tasks

We first describe a latent variable model for seq2seq tasks, which we call the Stochastic Switching-Ornstein-Uhlenbeck (SSOU) model. This model was introduced recently in biophysics [33] to describe the spontaneous oscillations of the tip of hair-cell bundles in the ear of the bullfrog. We consider observable sequences  $\mathbf{X} = (X_t)$  which are described by a one-dimensional stochastic process whose dynamics is driven by an autonomous latent stochastic process  $\mathbf{C} = (C_t)$  and a Gaussian white noise that is independent to  $C_t$ . Here and in the following we index sequences by a time variable  $t \geq 0$ , and use bold letters such as  $\mathbf{X}$  to denote sequences, or trajectories. A sequence of length  $T$  can be sampled from the stochastic differential equation

$$X_{t+1} - X_t = -\kappa(X_t - C_t)dt + \sqrt{2D}dB_t, \quad (1)$$

with  $t \in [0, T - 1]$ . Here,  $dB_t$  is the increment of the Wiener process in  $[t, t + dt]$ , with  $\langle dB_t \rangle = 0$  and  $\langle (dB_t)(dB_{t'}) \rangle = \delta(t - t')dt$ . The angled brackets  $\langle \cdot \rangle$  indicate an average over the noise process. We

denote the parameters  $D > 0$  and  $\kappa > 0$  as diffusion coefficient and trap stiffness for reasons described below.

A well-known application of eq. (1) in statistical physics is to describe the trajectories of a small particle (e.g. a colloid) in an aqueous solution undergoing Brownian motion [35] in a parabolic potential with time-dependent center  $C_t$ . Such physical model is often realized with microscopic particles immersed in water and trapped with optical tweezers [36–38]. When  $\kappa = 0$ , the particle is driven only by the noise term  $dW_t$  and performs a one-dimensional free diffusion along the real line with diffusion coefficient  $D$ . By choosing  $\kappa$  positive, the particle experiences a restoring force  $-\kappa(X_t - C_t)$  towards the instantaneous center of the potential. Such force  $F(X_t, C_t) = -\partial_X V(X, C)|_{X=X_t, C=C_t}$  tends to confine the particle to the vicinity of the point  $C_t$ , and is therefore often called a particle trap, which is modelled by a harmonic potential centred on  $C_t$

$$V(X_t, C_t) = \frac{\kappa}{2}(X_t - C_t)^2. \quad (2)$$

This motivates the name “stiffness” for  $\kappa$ ; the higher  $\kappa$ , the stronger the restoring force that confines the particle to the origin of the trap  $C_t$ .

The dynamics of  $X_t$  given by eq. (1) could be in principle driven by any stochastic process  $C_t$ . Here we focus on a minimal model where  $C_t = \{-1, 1\}$  is a dichotomous noise that changes sign after random waiting times that are drawn from a prescribed distribution. In particular, we will use a one-parameter family of gamma distributions (defined in eq. (6) below), which allows us to quantitatively control the degree of memory in the sequence of tokens  $\mathbf{C}$  in a simple manner. From a physical point of view, the dynamics of  $X_t$  consists in the alternate relaxation towards the two minima of the potential between consecutive switches, cf. fig. 1.

In what follows, we employ this setup as a seq2seq learning task where we aim to reconstruct the hidden sequence of trap positions  $\mathbf{C}$  given a sequence of particle positions  $\mathbf{X}$ , see fig. 1 for an illustration.

**The latent dynamics: switching the trap positions** The key idea in our model is to let the location of the potential  $C_t$  alternate in a stochastic manner between the two positions  $C_0 = \{-1, 1\}$ . The waiting time  $\tau$  spend in each of these two positions is drawn from the waiting-time distribution  $\psi_k(\tau)$ . For a generic choice of  $\psi_k(\tau)$ , the process  $C_t$  – and hence  $X_t$  – is non-Markovian and has a memory; we will discuss this in detail in section 4.1.

### 3 Methods

**Auto-regressive model** We first consider the arguably simplest machine-learning model that can be trained on sequential data, an auto-regressive model of order  $W$ ,  $\text{AR}(W)$ , see fig. 1. The output  $\hat{y} = (\hat{y}_t)$  of the model for the trap position given the sequence  $\mathbf{x}$  is given by

$$\hat{y}_t = \sigma \left( \sum_{\tau=1}^W w_\tau x_{t-\tau+1} + b \right) \quad (3)$$

where  $\sigma(x) = 1/(1 + e^{-x})$  is the sigmoidal activation function, and the weights  $w_\tau$  and the bias  $b$  are trained. We will also refer to the window size  $W \geq 1$  as the number of “memory units”, as it governs the number of tokens accessible to the model. We do not pad the input sequence, so the output sequence is shorter than the input sequence by  $W - 1$  steps.

**Convolutional two-layer network** The auto-regressive model can also be thought of as a single layer 1D convolutional neural network [39, 40] with a single filter and a kernel of size  $W$  with sigmoid activation. We also consider the natural extension of this model, CNN( $W$ ), a 1D convolutional neural network with two layers (see fig. 1). The first layer has the same kernel size ( $W$ ), but contains  $f$  filters with rectified linear activation [41]. In the second layer, we apply another convolution with a single filter and a kernel size of 1 with sigmoid activation. In this way, we can compare a CNN and an AR model with the same memory, i.e., same number of memory units ( $W$ ), and investigate the effect of additional nonlinearities of the second layer of the CNN on the prediction accuracy.

**Recurrent neural network** We also apply a recurrent network to this task that takes  $x_t$  as the input at step  $t$ , followed by a layer of Gated Recurrent Units [34] with a  $d$ -dimensional hidden state, followed by a fully connected layer with a single output and the sigmoid activation function (see fig. 1). We refer to this family of models by GRU( $d$ ).

**Generating the data set** We train all the models on a training set with  $N$  sequences  $\{\mathbf{x}^{(n)}\}_{n=1}^N$ , which can in principle be of different lengths. To obtain a sequence, we first generate a trajectory  $\mathbf{C}$  for the latent variable by choosing an initial condition at random from  $C_0 \in \{-1, 1\}$  and then drawing a sequence of waiting times from the distribution  $\psi_k(\tau)$ . Using the sampled trap positions,  $\mathbf{C}$ , we then sample the trajectory  $\mathbf{X}$  from eq. (1). Since in practice we do not have access to the full trajectory, as any experiment has a finite sampling rate, we subsample the process  $X_t$  by taking every  $s$ th element of the sequence. That is, for a given sequence  $\{X_t'\}_{t'=0}^{T'}$  of length  $T'$ , we construct a new sequence  $\mathbf{x} = (x_t)_{t=1}^T$ , where  $x_t = X_{s \times t}$  and  $T = \lfloor T'/s \rfloor$ . The subsampled sequence  $\mathbf{x}$  is then used as an input sequence. We verified that the finite time step for the integration of the SDE and the subsampling preserve the statistics of the continuum description that we use to derive our theoretical results, cf. appendix B.2.2. For convenience, we also introduce  $\mathbf{y} = (1 + \mathbf{c})/2$  to shift the trap position to 0 or 1. We then use this subsampled and shifted sequence of trap positions as the target.

**Training and evaluation** We train the models by minimising the mean squared loss function using Adam [42] with standard hyperparameters. For each sample sequence, the loss is defined as

$$\ell(\mathbf{y}_t, \hat{\mathbf{y}}_t) = \frac{1}{T - \tau_0} \sum_{\tau=\tau_0}^T (y_\tau - \hat{y}_\tau)^2, \quad (4)$$

where the offset  $\tau_0$  in the lower limit of the sum is necessary for the AR and CNN models since their output has a different length than the input sequence. For those models we choose  $\tau_0 = W - 1$ . For RNN models, however, we use  $\tau_0 = 1$  as the input and out sequence lengths are the same. We assess the performance of the trained models by first thresholding their outputs  $\hat{y}_t$  at 0.5 to obtain the sequence  $\hat{c}_t \in \{\pm 1\}$ , since the location of the centre of the potential has two possible values  $\pm 1$ . We then use the misclassification error  $\epsilon$  defined as

$$\epsilon = \frac{1}{N_{\text{samples}} N_\tau} \sum_{\text{samples}, \tau > \tau_h} \delta(c_\tau \neq \hat{c}_\tau), \quad (5)$$

where  $N_\tau$  is the length of the test sequence and  $\delta(x) = 1$  if the condition  $x$  is true and it is 0 otherwise, as the figure of merit throughout this work. Unless otherwise specified, we used 50000 training samples with mini-batch size 32 to train the models, and we evaluated them over 10000 test samples. To consistently compare different models with different output lengths and to reduce the boundary effects we only consider the predictions after an initial time offset  $\tau_h$ .

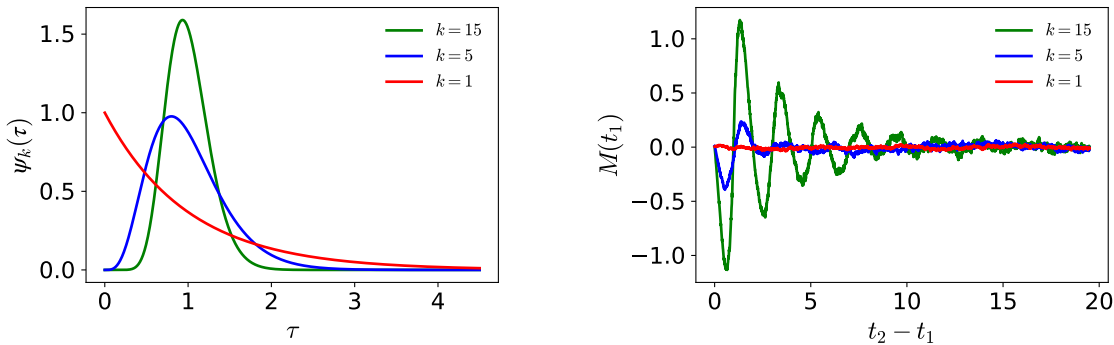


Figure 2: **Quantifying the memory of non-Markovian input sequences.** Left: waiting-time distribution  $\psi_k(\tau)$  given by eq. (6) for three choices of  $k$ . Right: measure  $M(t)$  (see eq. (8)) associated with the parameters in the left panel, which quantifies the memory of the past time  $t_1$  in the sequence. We obtain a memoryless sequence  $X_t$  with  $M(t) = 0$  by choosing  $k = 1$  which creates an exponential waiting-time distribution (6) (red curves). As the value of  $k$  increases, the memory becomes stronger (blue and green curves). *Parameters:*  $D = 0.5$ ,  $\kappa = 2$ ,  $\Omega_1 = \Omega_2 = [0.5, 1.5]$ ,  $t_3 - t_2 = 0.5$ , by generating  $N = 10^5$  trajectories via the Euler–Maruyama method [43] with simulation time step  $\Delta t = 5 \times 10^{-3}$ .

## 4 Results

### 4.1 The waiting time distribution of the trap controls the memory of the sequence

The key data property we would like to control is the memory of the sequence  $\mathbf{X}$ . In our SSOU model, the memory is controlled by tuning the memory in the latent sequence  $\mathbf{C}$ , which in turn depends on the distribution of the waiting time  $\tau$ . To fix ideas, we choose gamma-distributed waiting times,

$$\psi_k(\tau) = \frac{1}{\tau} \frac{(\tau k)^k e^{-k\tau}}{\Gamma(k)}, \quad (6)$$

where we set  $k \geq 1$ , while  $\Gamma(k) = \int_0^\infty dx x^{k-1} e^{-x}$  denotes the Gamma function. Note that for any choice of  $k$ , the normalization condition is  $\int_0^\infty \psi_k(\tau) d\tau = 1$  and the average waiting time between two consecutive switches is  $\langle \tau \rangle_k = \int_0^\infty \tau \psi_k(\tau) d\tau = 1$ . We can control the shape of the distribution by changing the value of  $k$ : the variance of the waiting time for example is  $k$ -dependent,  $\langle \tau^2 \rangle_k - \langle \tau \rangle_k^2 = 1/k$  (cf. fig. 2). Furthermore,  $k$  also controls the “degree of non-Markovianity” of the latent sequence  $\mathbf{C}$  as follows.

For the choice  $k = 1$ , the waiting-time distribution is exponential, making the process  $C_t$  Markovian. This result, together with the fact that eq. (1) is linear, implies that the observable process  $X_t$  is Markovian. Thus the probability distribution for the tokens  $x_t$  obeys the Markov identity [35]

$$p_{1|2}(x_{t_3}|x_{t_2}; x_{t_1}) = p_{1|1}(x_{t_3}|x_{t_2}), \quad (7)$$

where  $t_1 < t_2 < t_3$  represent different instants in time, and  $p_{1|m}$  denotes the conditional probability density (at one time instant) with  $m$  conditions (at  $m$  previous time instants). Equation (7) is the mathematical expression of the intuitive argument that we gave earlier: in a Markovian process, the future state  $x_{t_3}$  at time  $t_3$  given the state  $x_{t_2}$  at an earlier time  $t_2 < t_3$  is conditionally independent of the previous tokens  $x_{t_1}$  for all times  $t_1 < t_2$ .

However, most of the sequences analysed in machine learning are non-Markovian: in written language for example, the next word will not just depend on the previous word, but instead on a



large number of preceding words. We can generate non-Markovian sequences by choosing  $k > 1$ . To systematically investigate the impact of memory on the learning task, it is crucial to quantify the *degree* of non-Markovianity of the sequence for a given value of  $k$  beyond the binary distinction between Markovian and non-Markovian. Yet defining a practical measure that quantifies conclusively the degree of non-Markovianity is a non-trivial task [44, 45] and subject of ongoing research mainly done in the field of open quantum systems [46–50].

Here, we introduce a simple quantitative measure of the degree of non-Markovianity of the input sequence motivated directly by the Markov property (7),

$$M(t_1) \equiv \frac{\langle x_{t_3} | x_{t_2} \in \Omega_2, x_{t_1} \in \Omega_1 \rangle}{\langle x_{t_3} | x_{t_2} \in \Omega_2 \rangle} - 1 = \frac{\int_{\mathcal{X}} x_{t_3} p_{1|2}(x_{t_3} | x_{t_2} \in \Omega_2, x_{t_1} \in \Omega_1) dx_{t_3}}{\int_{\mathcal{X}} x_{t_3} p_{1|1}(x_{t_3} | x_{t_2} \in \Omega_2) dx_{t_3}} - 1. \quad (8)$$

Equation (8) involves crucially conditional expectations<sup>1</sup>, where the expectation of the future system state (at time  $t_3$ ) is conditioned on the present state (at time  $t_2$ ) or on the present and past state (at times  $t_2$  and  $t_1$ ). We have further introduced the notion of state space regions  $\Omega_1 \subseteq \mathcal{X}$  and  $\Omega_2 \subseteq \mathcal{X}$  which are subsets of the entire state space  $\mathcal{X} = \mathbb{R}$  that is accessible by the process  $\mathbf{X}$ . From eq. (7) it follows that for any Markovian process the measure  $M(t_1)$  (8) vanishes at all times, whereas  $M(t_1) \neq 0$  reveals the presence of non-Markovianity in the form of memory of the past time  $t_1$ . In a stationary process,  $M$  generally depends on the two time differences  $t_3 - t_2$  and  $t_2 - t_1$ , and on the choices of  $\Omega_1$  and  $\Omega_2$ . Here, we fix  $t_{2,3}$ ,  $\Omega_{1,2}$ , and vary  $t_1$ . To spot the non-Markovianity,  $t_3 - t_2$  should be comparable to the other time scales of the process. The choice of  $\Omega_1$  and  $\Omega_2$  is in principle arbitrary, but, for practical purposes, they should correspond to regions in the state space that are frequently visited.

We plot  $M(t_1)$  in fig. 2 for three different values of  $k$  obtained from numerical simulations of the SSOU. As expected, for a Markovian switching process with  $k = 1$ ,  $M(t_1)$  vanishes at all times  $t_1$ , while for  $k > 1$ ,  $M(t_1)$  displays non-zero values. The non-Markovianity measure  $M(t_1)$  defined in eq. (8) generally captures different facets of non-Markovianity. On the one hand, the decay with  $t_1$  measures how far the memory reaches into the past. On the other hand, the magnitude of  $M(t_1)$  tells us how much the predictability of the future given the present state profits from additionally knowing a past state. For the SSOU model, we observe in fig. 2 that increasing  $k$  increases both the decay time of  $M(t_1)$  and its amplitude, showing that that the parameter  $k$  controls conclusively the degree of non-Markovianity. We further note that  $M(t_1)$  displays oscillations for  $k > 1$ , reflecting the oscillatory behaviour of  $\mathbf{C}$  and  $\mathbf{X}$ , and that  $M(t_1)$  always decays to zero for sufficiently large values of  $t_2 - t_1$ , indicating the finite persistence time of the memory in the system. In conclusion of this analysis, we can in the following simply use  $k$  as control parameter of the degree of non-Markovianity of  $\mathbf{X}$ .

## 4.2 The performance of auto-regressive models

**The interplay between two time scales determines prediction accuracy** To gain some intuition, we first consider the simplest possible students, namely auto-regressive models AR(2) (3) with window size  $W = 2$ . The student predicts the value of  $c_t$  only using information about the present and the previous tokens  $x_t$  and  $x_{t-1}$ , giving it access to the current particle position and allowing it in principle also to estimate the velocity of the particle. We show the performance of this model obtained numerically in fig. 3. The accuracy of AR(2) varies significantly from less than 5% to essentially random guessing

<sup>1</sup>We denote  $\langle X | Y \in \Omega \rangle$  the conditional expectation of the random variable  $X$  given that the random variable  $Y$  satisfies a certain criterion, symbolized here as belonging to the set  $\Omega$ . Note that in general  $X$  and  $Y$  are statistically dependent, and that the conditioning may be done with respect to more than one random variables satisfying prescribed criteria.

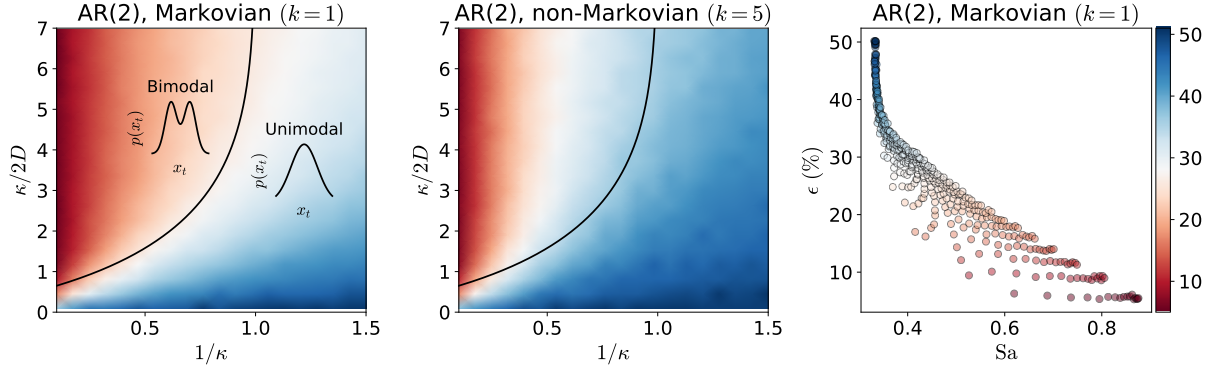


Figure 3: **Performance of auto-regressive AR(2) models for Markovian and non-Markovian sequences of the SSOU model across its “learnability phase diagram”.** (Left and middle) Reconstruction accuracy of the AR(2) model (in %) for different values of the diffusive time scale  $t_{\text{diff}} = 1/2D$  and the relaxation time  $t_{\kappa} = 1/\kappa$ , see eq. (9). We show these “phase diagrams” for Markovian sequences ( $k = 1$ ) and for non-Markovian sequences ( $k = 5$ ). In these diagrams, the two axes represent ratios of time scales,  $t_{\text{diff}}/t_{\kappa}$  (vertical axis) vs  $t_{\kappa}/\langle\tau\rangle_k = 1/\kappa$  (horizontal axis), since  $\langle\tau\rangle_k = 1$  for all  $k$ . (Right) Scatter plot of the error of several AR(2) models trained on Markovian sequences versus the Sarle coefficient (11), a measure of the bimodality of the distribution  $p(x_t)$ . *Parameters:* total simulation time for each parameter value  $\tau = 30$ , simulation time step  $\Delta t = 0.01$ , AR( $W$ ) window size  $W = 2$ ,  $\kappa$  varying from 0.1 to 0.6,  $\tau_h = 2$ , remaining training parameters as in fig. 1.

at 50% error as we vary the two time scales that influence the sequence statistics,

$$t_{\kappa} = 1/\kappa \quad \text{and} \quad t_{\text{diff}} = C_0^2/2D = 1/2D \quad (9)$$

the relaxation time and the diffusive time scale. The **relaxation time**  $t_{\kappa}$  determines how quickly the average position of the particle is restored to the centre of the trap when the the average waiting time  $\langle\tau\rangle_k = 1$ . A faster relaxation time means that the particle responds more quickly to a change in  $c_t$ , making reconstruction easier. The **diffusive time scale**  $t_{\text{diff}}$  sets the typical time that the system elapses to randomly diffuse a distance  $\sim |C_0|$ . The larger this time scale, the slower the particle moves randomly, as opposed to movement that follows the particle trap, hence improving the accuracy.

**A “phase diagram” for learnability** For memoryless sequences ( $k = 1$ ), we can explain this performance more quantitatively by solving for the data distribution  $p(x_t)$ . In particular, we observe that reconstructing the trap position is simplified when the marginal distribution of the particle distribution  $p(x_t)$  is bimodal, i.e. when it presents two well defined peaks around the trap centres  $\pm C_0$  (see fig. 3 top left). On the contrary, when the distribution  $p(x_t)$  is unimodal (corresponding to the case of fast relaxation times  $t_{\kappa}$ ) the learning performance worsens as the data is not sufficiently informative about the latent state  $\mathbf{C}$ . Interestingly, we observe that along the “phase boundary” between unimodal and bimodal the error is roughly homogeneous and approximately equal to 25%. The presence of two “phases” in terms of the bimodality/unimodality of the distribution  $p(x_t)$  is rationalised using recent analytical results [33] for the loci of the phase boundary in the the case  $k = 1$ , which is given by

$$\frac{t_{\text{diff}}}{t_{\kappa}} = \frac{(t_{\kappa} + 1/2) {}_1F_1(1/2, t_{\kappa} + 1/2, -t_{\text{diff}}/t_{\kappa})}{{}_1F_1(3/2, t_{\kappa} + 3/2, -t_{\text{diff}}/t_{\kappa})}. \quad (10)$$

This analytical result is obtained by finding the parameter values at which the derivative of  $p(x_t)$  at  $x_t = 0$  changes sign, which corresponds to a transition between unimodal and bimodal (see appendix A.1 for



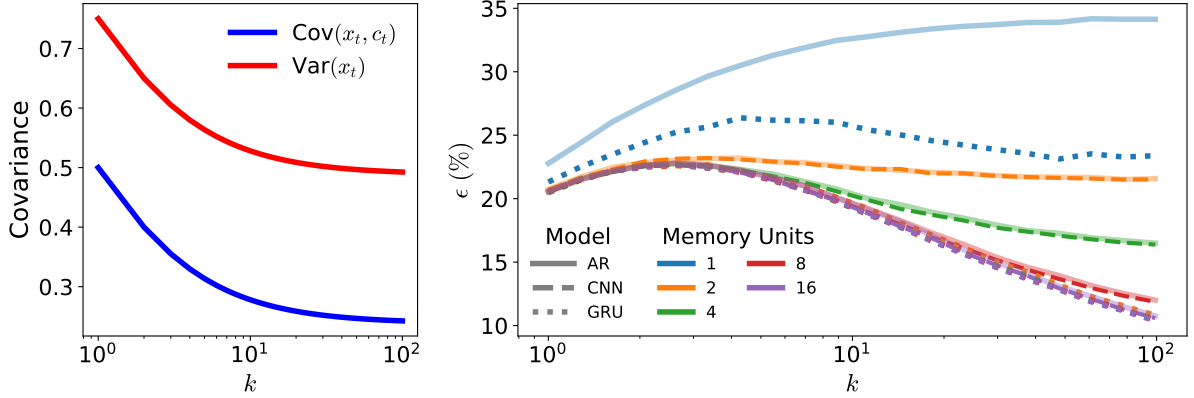


Figure 4: **The trade-off between student memory and sequence memory in recurrent neural networks and convolutional networks.** (Left) Analytical predictions for the covariance of the particle and trap position (12) in the non-Markovian case as a function of  $k$ . As we increase the non-Markovianity, correlations between  $x_t$  and  $c_t$  decay, complicating the reconstruction task. (Right) Prediction error  $\epsilon$  for students with different architectures: auto-regressive (AR), convolutional (CNN) and gated recurrent neural network (GRU). The memory units here correspond to the size of the kernel ( $W$ ) in the AR and the first layer of CNN models, and the number of units ( $d$ ) in the GRU models. The CNN models here all have  $f = 10$  filters in their first layer. *Parameters:* Similar to fig. 3 with  $\kappa = 2$ .

additional details). The line separating the two phases is drawn in black in the density plot of fig. 3. If we add memory to the sequence by choosing  $k > 1$ , an analytical solution for the phase boundary is challenging, yet we can explore the performance of the model with numerical simulations. Interestingly, when increasing the degree of memory to  $k = 5$  (see fig. 3 top right for  $k = 5$ ), we find that the AR(2) model yields a larger error than for  $k = 1$  Markovian sequences for all the parameter values explored in the learnability phase diagram. This means that not only that AR(2) is not able to extract all the available information from the sequence, but that the task has become harder by increasing  $k$ . We will explore further how the degree of non-Markovianity makes the task harder in the next section.

**Further statistical characterisation of the accuracy** We can further quantify the shape of the distribution by measuring the degree of bimodality using the Sarle coefficient [51],

$$\text{Sa} = (\sigma^2 + 1)/\mathcal{K} \quad (11)$$

with  $\sigma$  and  $\mathcal{K}$  the skewness and kurtosis of  $x_t$ , respectively. The Sarle coefficient takes values from 0 to 1 and is equal to 5/9 for the uniform distribution. Higher values may indicate bi-modality. We can see a clear correlation between the Sarle coefficient and the accuracy of the AR(2) model from the scatter plot on the right of fig. 3. Indeed, there appears to exist an upper bound on the accuracy in terms for the Sarle coefficient.

### 4.3 The interplay between sequence memory and model memory

**The statistical properties of the input sequence  $\mathbf{x}$  with memory** We saw in fig. 3 that increasing the sequence memory by increasing  $k$  makes the problem harder: the accuracy of the same student decreased. We can understand the root of this difficulty by studying the variance of the distribution  $p(x_t, c_t)$ . Using the tools introduced by Tucci *et. al.* [33], we can calculate these correlations analytically for any

integer  $k$ . As we describe in more detail in appendix A.2, we find that

$$\text{Var}(x_t) = \langle x_t^2 \rangle = \frac{D}{\kappa} C_0^2 + \kappa \sum_{n=0}^{k-1} Q_n \frac{k q_n - \kappa}{(k q_n)^2 - \kappa^2}, \quad (12a)$$

$$\text{Cov}(x_t, c_t) = \langle x_t c_t \rangle = 1 - \frac{2(1 + \kappa/k)^k - 1}{\kappa(1 + \kappa/k)^k + 1}, \quad (12b)$$

where  $Q_n \equiv -4(1 - q_n)/(k q_n)^2$ , and  $q_n \equiv 1 - e^{\pi(1+2n)/k}$  with  $n = 0, \dots, k-1$ ; we recall that  $\langle x_t \rangle = \langle c_t \rangle = 0$ . We plot both correlation functions as a function of  $k$  on the right of fig. 4. First, we note that the variance of the particle distribution decreases with  $k$  (red line). In other words, as we increase the memory of the sequence, the particle spends on average more time around the origin, making reconstruction harder. This is also born out by a decrease in the correlation between  $x_t$  and  $c_t$  (blue line). This loss in correlations is closely related to the error of the simplest reconstruction algorithm, where we estimate the particle positions  $\mathbf{c}$  by thresholding the particle position,  $c_t = \text{sign}(x_t)$ . As shown by a light blue line in the right panel of fig. 4, the error of this parameter-free, memoryless algorithm increases monotonically with  $k$ .

**Increasing memory in autoregressive models and convolutional neural networks** The existence of memory in the sequences suggests the use of students with larger memory to exploit these additional statistical dependencies. We first studied the performance of AR( $W$ ) models with varying  $W$ . As shown in fig. 4, we observed that for a fixed  $k$  increasing  $W$  generally helps with reducing the error  $\epsilon$  (solid lines), so models with larger memory can take advantage of the additional temporal correlations in the sequence and make better predictions in the large  $k$  limit. For the convolutional networks described in section 3 with  $f = 10$  filters (dashed lines), we observe that the additional filters and non-linearities in the CNN do not help with the predictions. We conclude that it is truly the memory that makes a difference on this data set and that even a simple AR model can completely take advantage of the information in a given time window.

**Recurrent neural networks** We numerically studied the performance of a gated recurrent unit GRU( $d$ ) [34] with hidden state size  $d$ , which can be thought of as a slightly more streamlined variant of the classic long short-term memory [52]. Although such an RNN reads in the input sequence one token at a time, it can build up long-time memory by continuously updating its internal state  $\mathbf{h} \in \mathbb{R}^d$ , cf. fig. 1. We show the test performance of GRU models with various internal state sizes  $d$  in fig. 4. The GRU display a good performance: as soon as the GRU( $d$ ) has a hidden state with a hidden state of dimension  $d = 2$ , it captures all the memory of the sequence at all  $k$ , achieving the limiting performance of AR( $W$ ) models with the largest window size. Indeed, the error curves for GRUs with  $d \geq 2$  all coincide. This observation, together with the limited performance gain from increasing  $W$  in the AR( $W$ ) and CNN( $W$ ) models suggest that the error is approaching the Bayes limit. Note that the rate of this convergence depends on  $k$ , since the student memory required to achieve the optimal performance depends on the degree of non-Markovianity of the sequence (see Fig. 4).

**The interplay between sequence memory and model memory** Finally, we found that for all three architectures – AR, CNN and GRU – there is a peak in the reconstruction error, usually around  $k \approx 5$ . This peak can be understood by noting that the tokens  $x_t$  get more concentrated around the origin as  $k$  is increased, as we have shown in eq. (12). Therefore,  $x_t$  is less correlated with  $c_t$  in the highly non-Markovian limit. However, as the degree of non-Markovianity is increased through increasing  $k$ , the history of the tokens position  $x_t$  can help with predicting the trap’s position  $c_t$  more accurately.

The trade-off between these two phenomena is evident in the non-monotonous dependency of the error as a function of  $k$  for models with larger memory in fig. 4. For small  $k$ , the correlation between different times in the sequence is not strong enough to compensate the loss of information about the trap’s position in the signal, but for larger  $k$  the trap’s position is more regular and the history of  $x_t$  can be used to infer the  $c_t$  more efficiently.

## 5 Concluding perspectives

We have introduced the stochastically switching Ornstein-Uhlenbeck process (SSOU) to model seq2seq machine learning tasks. This model gives us precise control over the memory of the generated sequences, which we used to study the interaction between this memory and various machine learning models trained on this data, ranging from simple auto-regressive models to convolutional and recurrent neural networks. We found that the accuracy of these models is governed by the interaction of the different time scales of the data, and we discovered an intriguing interplay between the memory of the students and the sequence which leads to non-monotonic error curves.

An important limitation of the SSOU model considered here is that it only allows one to study correlations that decay exponentially fast. As a next step it would be interesting to explicitly consider the impact of long-range memory in the data sequence. This could be implemented in the SSOU model e.g. by choosing a long-ranged waiting time distribution, such as a power law. Another limitation concerns the linearity of the model analysed here. We speculate that a nonlinear model could provide insights into the different ways AR and CNN utilise the data. In our model, one could implement a tunable nonlinearity by adding a non-quadratic term of increasing amplitude to the trap potentials, eq. (2). Similarly, to enrich the statistical dependencies within the sequence, one could generate non-symmetric sequences with respect to a  $x \rightarrow -x$  sign inversion, by implementing two different waiting times. It would also be intriguing to analyse the impact of sequence memory on the dynamics of simple RNN models [53, 54], such as those with low-rank connectivity [55, 56].

Finally, it would be intriguing to apply some of the neural networks studied here to noisy non-Markovian signals extracted from experiments in physical or biological systems [57–63]. Examples include the recent application of the SSOU to infer the thermodynamics of spontaneous oscillations of the hair-cell bundles in the ear of the bullfrog [33] or the characterisation and mitigation the effects of non-Markovian noise [64, 65].

## Acknowledgements

We thank Roman Belousov, Alessandro Ingrosso, Stéphane d’Ascoli, Andrea Gambassi, Florian Berger, Gogui Alonso, AJ Hudspeth, Aljaz Godec and Jyrki Piilo for stimulating discussions. A.S. is supported by a Chicago Prize Postdoctoral Fellowship in Theoretical Quantum Science.

## References

1. Vaswani, A. *et al.* *Attention is All you Need* in *Advances in Neural Information Processing Systems* (eds Guyon, I. *et al.*) **30** (2017).
2. Valipour, M., You, B., Panju, M. & Ghodsi, A. SymbolicGPT: A Generative Transformer Model for Symbolic Regression. *arXiv preprint arXiv:2106.14131* (2021).
3. Kamienny, P.-A., d’Ascoli, S., Lample, G. & Charton, F. End-to-end symbolic regression with transformers. *arXiv preprint arXiv:2204.10532* (2022).
4. Biggio, L., Bendinelli, T., Neitz, A., Lucchi, A. & Parascandolo, G. *Neural Symbolic Regression that Scales* in *International Conference on Machine Learning* (2021), 936–945.
5. He, S. *et al.* *Image captioning through image transformer* in *Proceedings of the Asian Conference on Computer Vision* (2020).
6. Dosovitskiy, A. *et al.* *An Image is Worth 16x16 Words: Transformers for Image Recognition at Scale* in *International Conference on Learning Representations* (2021).
7. Touvron, H. *et al.* *Training data-efficient image transformers & distillation through attention* in *International Conference on Machine Learning* (2021), 10347–10357.
8. Gardner, E. & Derrida, B. Three unfinished works on the optimal storage capacity of networks. *Journal of Physics A: Mathematical and General* **22**, 1983 (1989).
9. Seung, H. S., Sompolinsky, H. & Tishby, N. Statistical mechanics of learning from examples. *Physical review A* **45**, 6056 (1992).
10. Engel, A. & Van den Broeck, C. *Statistical mechanics of learning* (Cambridge University Press, 2001).
11. Carleo, G. *et al.* Machine learning and the physical sciences. *Reviews of Modern Physics* **91**, 045002 (2019).
12. Krizhevsky, A., Sutskever, I. & Hinton, G. *Imagenet classification with deep convolutional neural networks* in *Advances in neural information processing systems* (2012), 1097–1105.
13. Simonyan, K. & Zisserman, A. *Very Deep Convolutional Networks for Large-Scale Image Recognition* in *International Conference on Learning Representations* (2015).
14. He, K., Zhang, X., Ren, S. & Sun, J. *Deep residual learning for image recognition* in *Proceedings of the IEEE conference on computer vision and pattern recognition* (2016), 770–778.
15. Pope, P., Zhu, C., Abdelkader, A., Goldblum, M. & Goldstein, T. *The Intrinsic Dimension of Images and Its Impact on Learning* in *International Conference on Learning Representations* (2021).
16. Chung, S., Lee, D. D. & Sompolinsky, H. Classification and Geometry of General Perceptual Manifolds. *Phys. Rev. X* **8**, 031003 (3 2018).
17. Goldt, S., Mézard, M., Krzakala, F. & Zdeborová, L. Modeling the influence of data structure on learning in neural networks: The hidden manifold model. *Phys. Rev. X* **10**, 041044 (2020).
18. Goldt, S. *et al.* *The Gaussian equivalence of generative models for learning with shallow neural networks* in *Proceedings of the 2nd Mathematical and Scientific Machine Learning Conference* (eds Bruna, J., Hesthaven, J. & Zdeborová, L.) **145** (PMLR, 2022), 426–471.
19. Ghorbani, B., Mei, S., Misiakiewicz, T. & Montanari, A. *When do neural networks outperform kernel methods?* in *Advances in Neural Information Processing Systems* **33** (2020).

20. Richards, D., Mourtada, J. & Rosasco, L. *Asymptotics of Ridge(less) Regression under General Source Condition in Proceedings of The 24th International Conference on Artificial Intelligence and Statistics* (eds Banerjee, A. & Fukumizu, K.) **130** (PMLR, 2021), 3889–3897.
21. Chizat, L. & Bach, F. *Implicit bias of gradient descent for wide two-layer neural networks trained with the logistic loss in Conference on Learning Theory* (2020), 1305–1338.
22. Refinetti, M., Goldt, S., Krzakala, F. & Zdeborová, L. *Classifying high-dimensional Gaussian mixtures: Where kernel methods fail and neural networks succeed in Proceedings of the 38th International Conference on Machine Learning* (eds Meila, M. & Zhang, T.) **139** (PMLR, 2021), 8936–8947.
23. Loureiro, B. *et al.* Learning Gaussian Mixtures with Generalized Linear Models: Precise Asymptotics in High-dimensions. *Advances in Neural Information Processing Systems* **34** (2021).
24. Harsh, M., Tubiana, J., Cocco, S. & Monasson, R. ‘Place-cell’ emergence and learning of invariant data with restricted Boltzmann machines: breaking and dynamical restoration of continuous symmetries in the weight space. *Journal of Physics A: Mathematical and Theoretical* **53**, 174002 (2020).
25. Favero, A., Cagnetta, F. & Wyart, M. Locality defeats the curse of dimensionality in convolutional teacher-student scenarios. *Advances in Neural Information Processing Systems* **34** (2021).
26. Ingrosso, A. & Goldt, S. Data-driven emergence of convolutional structure in neural networks. *arXiv preprint arXiv:2202.00565* (2022).
27. Spigler, S., Geiger, M. & Wyart, M. Asymptotic learning curves of kernel methods: empirical data versus teacher–student paradigm. *Journal of Statistical Mechanics: Theory and Experiment* **2020**, 124001 (2020).
28. d’Ascoli, S., Gabrié, M., Sagun, L. & Biroli, G. *On the interplay between data structure and loss function in classification problems in Advances in Neural Information Processing Systems* (eds Ranzato, M., Beygelzimer, A., Dauphin, Y., Liang, P. & Vaughan, J. W.) **34** (Curran Associates, Inc., 2021), 8506–8517.
29. Benna, M. K. & Fusi, S. Place cells may simply be memory cells: Memory compression leads to spatial tuning and history dependence. *Proceedings of the National Academy of Sciences* **118**, e2018422118 (2021).
30. Gerace, F., Saglietti, L., Mannelli, S. S., Saxe, A. & Zdeborová, L. Probing transfer learning with a model of synthetic correlated datasets. *Machine Learning: Science and Technology* **3**, 015030 (2022).
31. Bach, F. Breaking the curse of dimensionality with convex neural networks. *The Journal of Machine Learning Research* **18**, 629–681 (2017).
32. Ghorbani, B., Mei, S., Misiakiewicz, T. & Montanari, A. *Limitations of Lazy Training of Two-layers Neural Network in Advances in Neural Information Processing Systems* **32** (2019), 9111–9121.
33. Tucci, G. *et al.* Modelling Active Non-Markovian Oscillations. *arXiv preprint arXiv:2201.12171* (2022).
34. Cho, K., van Merriënboer, B., Bahdanau, D. & Bengio, Y. *On the Properties of Neural Machine Translation: Encoder–Decoder Approaches in Proceedings of SSST-8, Eighth Workshop on Syntax, Semantics and Structure in Statistical Translation* (2014), 103–111.
35. Van Kampen, N. G. *Stochastic processes in physics and chemistry* (Elsevier, 1992).
36. Martinez, I. A. & Petrov, D. Force mapping of an optical trap using an acousto-optical deflector in a time-sharing regime. *Applied optics* **51**, 5522–5526 (2012).

37. Pietzonka, P., Ritort, F. & Seifert, U. Finite-time generalization of the thermodynamic uncertainty relation. *Physical Review E* **96**, 012101 (2017).
38. Martínez, I. A., Roldán, E., Parrondo, J. M. & Petrov, D. Effective heating to several thousand kelvins of an optically trapped sphere in a liquid. *Physical Review E* **87**, 032159 (2013).
39. LeCun, Y. *et al.* Backpropagation Applied to Handwritten Zip Code Recognition. *Neural Computation* **1**, 541–551 (1989).
40. Goodfellow, I., Bengio, Y. & Courville, A. *Deep learning* (MIT press, 2016).
41. Fukushima, K. Visual Feature Extraction by a Multilayered Network of Analog Threshold Elements. *IEEE Transactions on Systems Science and Cybernetics* **5**, 322–333 (1969).
42. Kingma, D. P. & Ba, J. Adam: A method for stochastic optimization. *arXiv preprint arXiv:1412.6980* (2014).
43. Kloeden, P. E. & Platen, E. in *Numerical Solution of Stochastic Differential Equations* 103–160 (Springer, 1992).
44. Lapolla, A. & Godec, A. Toolbox for quantifying memory in dynamics along reaction coordinates. *Physical Review Research* **3**, L022018 (2021).
45. Lapolla, A. & Godec, A. Manifestations of projection-induced memory: General theory and the tilted single file. *Frontiers in Physics* **7**, 182 (2019).
46. Laine, E.-M., Piilo, J. & Breuer, H.-P. Measure for the non-Markovianity of quantum processes. *Physical Review A* **81**, 062115 (2010).
47. Hall, M. J., Cresser, J. D., Li, L. & Andersson, E. Canonical form of master equations and characterization of non-Markovianity. *Physical Review A* **89**, 042120 (2014).
48. Rivas, Á., Huelga, S. F. & Plenio, M. B. Entanglement and non-Markovianity of quantum evolutions. *Physical review letters* **105**, 050403 (2010).
49. Huang, Z., Guo, X.-K. *et al.* Quantifying non-Markovianity via conditional mutual information. *Physical Review A* **104**, 032212 (2021).
50. Strasberg, P. & Esposito, M. Response functions as quantifiers of non-Markovianity. *Physical review letters* **121**, 040601 (2018).
51. Ellison, A. M. Effect of seed dimorphism on the density-dependent dynamics of experimental populations of *Atriplex triangularis* (Chenopodiaceae). *American Journal of Botany* **74**, 1280–1288 (1987).
52. Hochreiter, S. & Schmidhuber, J. Long short-term memory. *Neural computation* **9**, 1735–1780 (1997).
53. Sompolinsky, H., Crisanti, A. & Sommers, H.-J. Chaos in random neural networks. *Physical review letters* **61**, 259 (1988).
54. Sussillo, D. & Abbott, L. F. Generating coherent patterns of activity from chaotic neural networks. *Neuron* **63**, 544–557 (2009).
55. Mastrogiuseppe, F. & Ostojic, S. Linking connectivity, dynamics, and computations in low-rank recurrent neural networks. *Neuron* **99**, 609–623 (2018).
56. Schuessler, F., Mastrogiuseppe, F., Dubreuil, A., Ostojic, S. & Barak, O. The interplay between randomness and structure during learning in RNNs. *Advances in neural information processing systems* **33**, 13352–13362 (2020).
57. Mindlin, G. B. Nonlinear dynamics in the study of birdsong. *Chaos* **27**, 092101 (2017).



58. Vettoretti, G. & Peltier, W. R. Fast physics and slow physics in the nonlinear Dansgaard–Oeschger relaxation oscillation. *J. Clim.* **31**, 3423 (2018).
59. Cavallaro, M. & Harris, R. J. Effective bandwidth of non-Markovian packet traffic. *Journal of Statistical Mechanics: Theory and Experiment* **2019**, 083404 (2019).
60. Roldán, É., Barral, J., Martin, P., Parrondo, J. M. & Jülicher, F. Quantifying entropy production in active fluctuations of the hair-cell bundle from time irreversibility and uncertainty relations. *New Journal of Physics* **23**, 083013 (2021).
61. Belousov, R., Berger, F. & Hudspeth, A. Volterra-series approach to stochastic nonlinear dynamics: Linear response of the Van der Pol oscillator driven by white noise. *Phys. Rev. E* **102**, 032209 (2020).
62. Brückner, D. B. *et al.* Stochastic nonlinear dynamics of confined cell migration in two-state systems. *Nat. Phys.* **15**, 595 (2019).
63. Skinner, D. J. & Dunkel, J. Estimating Entropy Production from Waiting Time Distributions. *Phys. Rev. Lett.* **127**, 198101 (19 2021).
64. Mavadia, S., Frey, V., Sastrawan, J., Dona, S. & Biercuk, M. J. Prediction and real-time compensation of qubit decoherence via machine learning. *Nature communications* **8**, 1–6 (2017).
65. Majumder, S., Andreta de Castro, L. & Brown, K. R. Real-time calibration with spectator qubits. *npj Quantum Information* **6**, 1–9 (2020).
66. Glorot, X. & Bengio, Y. *Understanding the difficulty of training deep feedforward neural networks* in *Proceedings of the thirteenth international conference on artificial intelligence and statistics* (2010), 249–256.

## A Analytical details

### A.1 Details on the calculation of the phase diagram

As anticipated in section 4.1, the process  $C_t$  becomes Markovian in the case of exponentially distributed waiting time distribution; in our units this coincides with  $\psi_{k=1}(\tau) = e^{-\tau}$ . For this simple case, one can characterise analytically the mono-bistable transition of the stationary density  $p(x_t)$ . This can be done by looking at the behaviour of  $p(x_t)$  at the origin: if  $x_t = 0$  is a point of maximum,  $p(x_t)$  is unimodal, bimodal otherwise. We report from [33] the explicit expression of  $p(x_t)$ , which reads

$$p(x_t) = \frac{1}{\sqrt{\pi}} \frac{\Gamma(\zeta + \frac{1}{2})}{\Gamma(\zeta - \frac{1}{2})} \int_{-1}^{+1} dz \frac{e^{-\chi(x_t-z)^2}}{\sqrt{\pi/\chi}} (1-z^2)^{\zeta-1}, \quad (\text{A.1})$$

where we have set  $C_0 = 1$ , and we have defined the dimensionless parameters  $\zeta = t_\kappa / \langle \tau \rangle_k = 1/\kappa$  and  $\chi = t_{\text{diff}}/t_\kappa = \kappa/(2D)$ . One finds that  $x_t = 0$  is an extremum point for  $p(x_t)$ , coinciding with the condition  $p'(0) = 0$ . The nature of  $x_t = 0$  is understood by looking at the second derivative of  $p(x_t)$ , that is

$$p''(0) = \frac{2}{\sqrt{\pi/\chi^3}} \left[ \frac{\chi}{\zeta + 1/2} {}_1F_1\left(\frac{3}{2}, \zeta + \frac{3}{2}, -\chi\right) - {}_1F_1\left(\frac{1}{2}, \zeta + \frac{1}{2}, -\chi\right) \right], \quad (\text{A.2})$$

where  ${}_1F_1$  denotes the confluent hypergeometric function. The mono-bimodal transition occurs upon crossing the critical value  $\chi^*$  satisfying the condition  $p''(0) = 0$ , or equivalently, eq. (10). For  $\chi < \chi^*$ , the second derivative  $p''(0)$  is negative and  $p(x)$  is unimodal, while it is bimodal otherwise.

### A.2 Computation of the correlation functions in the non-Markovian case

In this section, we report the analytical expression for the (stationary) auto-correlation function  $\mathcal{C}_X(t)$  of the process  $X_t$  in eq. (1), and its Fourier transform, i.e., the power spectral density (PSD)  $S_X(\omega)$ . For Gamma-distributed waiting-time  $\psi_k(\tau)$  as given in eq. (6), the PSD  $S_X(\omega)$  of the process  $X_t$  is given by [33]

$$S_X(\omega) = \frac{2D + \kappa^2 S_C(\omega)}{\kappa^2 + \omega^2}, \quad (\text{A.3})$$

where  $S_C(\omega)$  denotes the PSD of the process  $C_t$ , whose explicit expression reads

$$S_C(\omega) = \frac{4C_0^2}{\omega^2} \frac{R^2(\omega) - 1}{R^2(\omega) + 1 + 2R(\omega) \cos \phi(\omega)}, \quad (\text{A.4})$$

with  $R(\omega) = [1 + (\omega/k)^2]^{k/2}$ , and  $\phi(\omega) = k \arctan(\omega/k)$ . According to the Wiener-Khinchin theorem [35], the inverse Fourier transform of  $S_C(\omega)$  and  $S_X(\omega)$  coincides with the auto-correlation functions  $\mathcal{C}_C(t) \equiv \lim_{\tau \rightarrow \infty} \langle C_{t+\tau} C_\tau \rangle$  and  $\mathcal{C}_X(t) \equiv \lim_{\tau \rightarrow \infty} \langle X_{t+\tau} X_\tau \rangle$ . In the case of integer  $k$ , their expressions can be calculated explicitly according to

$$\mathcal{C}_C(t) = C_0^2 \sum_{n=0}^{k-1} Q_n e^{-t k q_n}, \quad (\text{A.5})$$

$$\mathcal{C}_X(t) = \frac{D}{\kappa} e^{-\kappa t} + C_0^2 \kappa \sum_{n=0}^{k-1} Q_n \frac{k q_n e^{-\kappa t} - \kappa e^{-k q_n t}}{(k q_n)^2 - \kappa^2}, \quad (\text{A.6})$$

where  $Q_n \equiv -4(1 - q_n)/(k q_n)^2$ , and  $q_n \equiv 1 - e^{\pi(1+2n)/k}$  with  $n = 0, \dots, k-1$ ; in fig. 5, we compare eq. (A.6) with the numerical estimate of  $\mathcal{C}_X$  for three different choices of  $k$ . Note that the value of the sum  $\sum_{n=0}^{k-1} Q_n = 1$  implies the correct initial condition  $C_c(0) = C_0^2$ . Moreover, one can deduce the

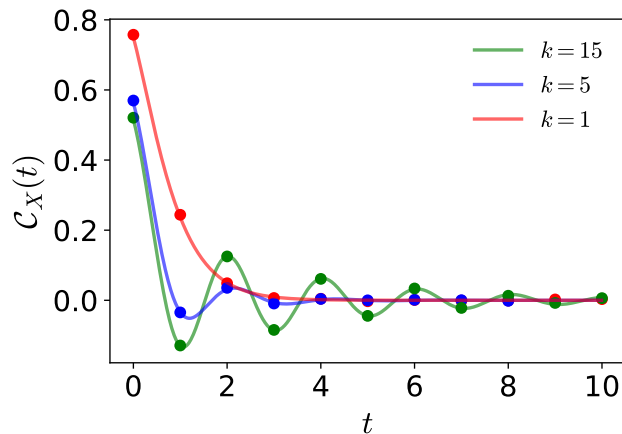


Figure 5: **Autocorrelation function of the process  $C_t$ .** We compare the analytical formula of  $C_X(t)$  in eq. (A.5) (solid line) with its numerical prediction (circles), calculated by generating  $N = 5 \times 10^4$  trajectories via Euler–Maruyama method with  $\Delta t = 0.01$ ,  $\kappa = 2$ ,  $D = 0.5$  and various values of  $k$ .

stationary expression of the stationary variance  $\langle x_t^2 \rangle$  of the process  $X_t$  from the initial value  $C_X(0)$ . We conclude this section by reporting the value of the covariance  $\langle x_t c_t \rangle$ , which we derive here using similar methods as those in ref. [33], and is given by

$$\langle x_t c_t \rangle = 1 - \frac{2 (1 + \kappa/k)^k - 1}{\kappa (1 + \kappa/k)^k + 1}. \quad (\text{A.7})$$

## B Additional experimental results

We use a fixed number of 40 epochs and do not perform any hyperparameter tuning (with the exception of the GRU(1) model as detailed in Appendix B) as the models are rather simple and varying these parameters have negligible effects on the results.

### B.1 Additional details on creating the figures

In this section, we provide additional details on the generation of some of the figures of the main text.

**Figure 3** The parameter sweep in the top left and top right panels was done by inspecting the intervals  $\kappa \in [2/3, 10]$  and  $D \in [1/21, 50]$  in a regular grid of size  $20 \times 20$ . We used a finite-sample estimate for Sarle’s coefficient given by  $(\sigma^2 + 1)/(3 + \omega\mathcal{K})$ , with  $\sigma$  the skewness and  $\mathcal{K}$  the kurtosis of the sequence  $\mathbf{X}$ , and  $\omega = (T - 1)^2/(T - 2)(T - 3)$  and  $T = \tau/\Delta t = 3 \times 10^3$ .

### B.2 Ensuring the consistency between continuous-time theory and sampled sequences

Here we discuss how we ensured that our theory that is based on the continuous-time description of the stochastic processes  $X_t$  and  $C_t$  (cf. section 2) and the sequences we find into the machine learning models are consistent. If the sequence is sampled with a very small time step, the student almost never sees a jump of the trap, and effectively samples from an (equilibrium) distribution in one trap. On the other hand, in the limit of very large time steps, the temporal correlations in the sequence is not visible, e.g., recall that the non-Markovianity parameter eventually decays to zero for infinitely large time differences. Thus, it is crucial to sample with a time step that is smaller but comparable to the

characteristic time scales of the data sequence. In practice, one would thus need to estimate those time scales in a preceding data analysis step, before feeding the data into the network. For this purpose, a suitable method is to compute the autocorrelation function of the input sequence data which reveals the time scales. For the SSOU model, we provide the analytical expression for the correlation function in eq. (12). For the SSOU, the characteristic time scales are given by the oscillation period and the decay time of the autocorrelation function, which are of order of magnitude 1 for our parameter choice (see fig. 5).

### B.2.1 Correlations function and integration time step

To generate trajectories with correct statistics we vary the time differences  $\Delta t$ , which corresponds to the discrete version of  $dt$  in numerically integrating eq. (1). We find that  $\Delta t = 0.005$  reproduces the correct statistics in fig. 5.

### B.2.2 The role of subsampling

As mentioned earlier the trajectories are first generated by numerically integrating eq. (1) by choosing a sufficiently small  $dt$  such that the statistical properties of the trajectories match their theoretical values, which we verified by checking the correlation functions estimated analytically match our theoretical result (see fig. 5).

As we discuss in the main text, we subsample the full trajectories before training the machine learning models. This subsampling also simplifies the optimization and accelerates the training. However, in doing so, we need to make sure that the qualitative properties of the model remain unchanged. Therefore, we compare AR models trained on the original trajectories with those trained on subsampled trajectories. We observe that the key properties of the problem, namely the strictly increasing errors with  $k$  in the memoryless learning ( $W = 1$ ), and non-monotonic behaviour of errors due to the trade-off between the memory ( $W$ ) and the non-Markovianity ( $k$ ) in more complicated models are preserved.

As mentioned in the main text we subsample the sequences by taking every  $s$ th element of the original sequence in the dataset when training the models in Sec. 4.3. To investigate the effect of this subsampling we compare AR models trained on original dataset with those trained on subsampled sequences with  $s = 30$ , and show the results in fig. 6. The qualitative features of the error curves as a function of non-Markovianity  $k$  are preserved. The monotonicity of errors for memoryless models and the trade-off between improvements by memory and the difficulty of correlating the particle's position  $x_t$  to the trap's position  $c_t$ , the two main features of fig. 4, are present in both the original and the subsampled cases.

## B.3 The thresholding algorithm

As a baseline benchmark, we consider a simple thresholding algorithm, where  $\hat{c}_t = \text{sgn}(x_t)$ . Put simply, this algorithm infers the potential's location by only considering the position of the particle at a single point  $x_t$  and choose the closest configuration of potential  $c_t$  to that position. In fig. 7 we compare the performance of the AR(1) model with the thresholding algorithm and observe that AR(1) matches the performance of the the thresholding algorithm.

## B.4 Selecting the best GRU(1) model

To find the best performing GRU(1) we train model for all  $k$  values shown in fig. 4 we train five different instance of the network initialized randomly using as suggested in Ref. [66]. We choose the best

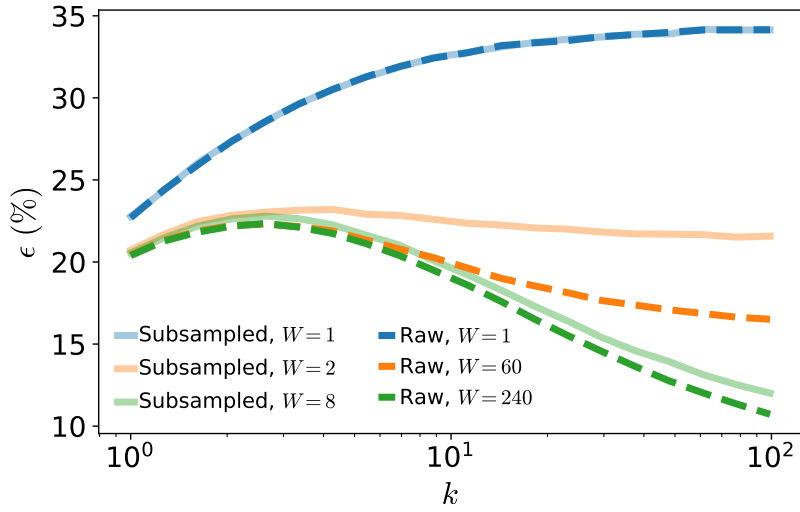


Figure 6: **Subsampling effects.** We compare the error of AR models trained on original raw dataset and the subsampled one with a subsampling factor of  $s = 30$ . The key qualitative features of the error curves as function of the non-Markovianity  $k$  are not affected by subsampling.

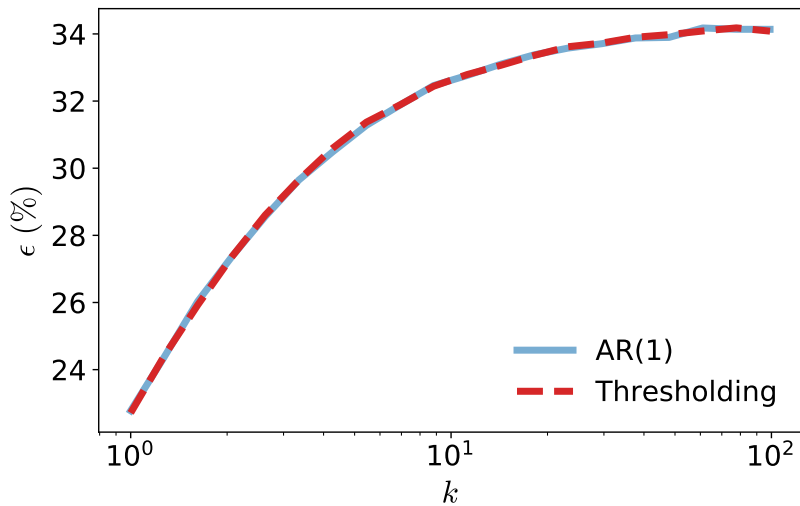


Figure 7: **Comparing the AR(1) and the thresholding algorithm.** Both the AR(1) model and the thresholding algorithm only have access to the position of the particle at a single point. As a consistency check we compare the performance of the two and observe that they match.

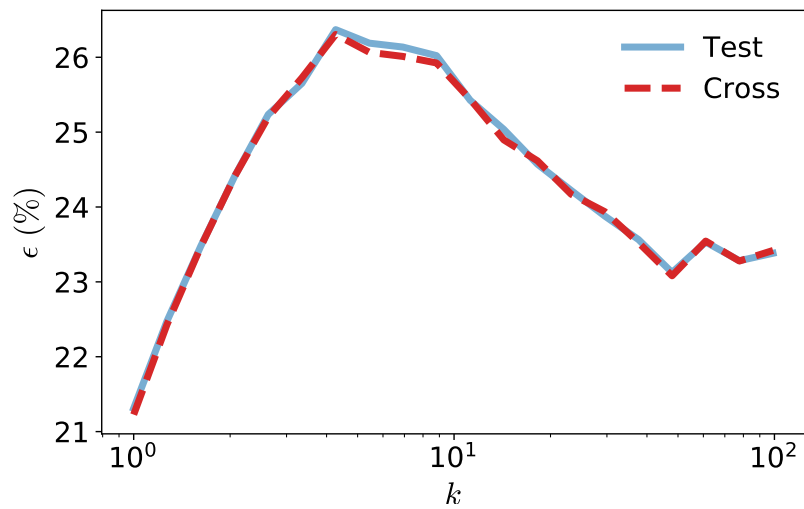


Figure 8: **Validating the GRU(1) model.** The accuracy of the best performing GRU(1) models over the cross validation and test sets match.

performing model over 10000 samples for each  $k$ , and report the accuracy on a new set of 10000 samples. As shown in fig. 8 the test and cross validation accuracy are in excellent agreement.